THE JOURNAL OF PHYSICAL CHEMISTRY Letters

Letter

pubs.acs.org/JPCL

Toward Ab Initio Optical Spectroscopy of the Fenna–Matthews–Olson Complex

Daniel J. Cole,*[,†,‡] Alex W. Chin,[†] Nicholas D. M. Hine,[†,§] Peter D. Haynes,[§] and Mike C. Payne[†]

[†]TCM Group, Cavendish Laboratory, 19 JJ Thomson Ave, Cambridge CB3 0HE, United Kingdom

[‡]Department of Chemistry, Yale University, 225 Prospect Street, New Haven, Connecticut 06520-8107, United States

[§]Departments of Materials and Physics, Imperial College London, Exhibition Road, London SW7 2AZ, United Kingdom

Supporting Information

ABSTRACT: We present progress toward a first-principles parametrization of the Hamiltonian of the Fenna–Matthews–Olson pigment–protein complex, a molecule that has become key to understanding the role of quantum dynamics in photosynthetic exciton energy transfer. To this end, we have performed fully quantum mechanical calculations on each of the seven bacteriochlorophyll pigments that make up the complex, including a significant proportion of their protein environment (more than 2000 atoms), using linear-scaling density functional theory exploiting a recent development for the computation of excited states. Local pigment transition energies and interpigment coupling between optical transitions have been calculated and are in good agreement with the literature consensus. Comparisons between simulated and experimental optical spectra point toward future work that may help to elucidate important design principles in these nanoscale devices.

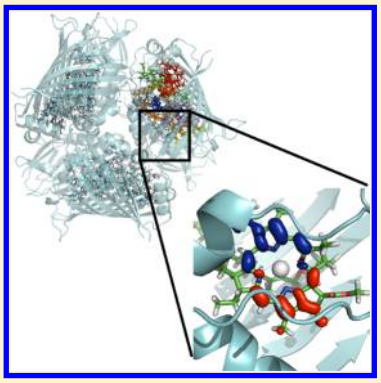

SECTION: Spectroscopy, Photochemistry, and Excited States

The Fenna–Matthews–Olson (FMO) complex is an important pigment–protein complex (PPC) in the molecular apparatus that drives photosynthesis in green sulfur bacteria.[1−3] Functioning as a linker complex, its role is to funnel electronic excitations (excitons) created by ambient photon absorption in the antenna complexes (chlorosomes) toward the reaction centers, where their excitation energy is used to generate free charges for chemical use. In the low-light environment in which many strains of green sulfur bacteria are found, the internal quantum efficiency of photon-to-electron conversion often approaches 100%, making the mechanisms that drive their photosynthetic apparatus of potential interest for research into organic molecule-based devices for solar energy transduction.[4−6]

The FMO complex is rare in being water-soluble and was the first PPC structure to be resolved by X-ray spectroscopy. (The most recent structure has a resolution of 1.3 Å.)[7] This revealed a relatively simple structure, consisting of a trimeric unit in which each monomer contains just seven bacteriochlorophyll (BChla) molecules. These constitute the optically active pigments (chromophores) of the complex that carry the exciton energy and are bound and coordinated in space by noncovalent interactions with the surrounding protein. The resolved, few-chromophore structure of FMO, together with its readily probeable absorption spectra, make it a very attractive system for theoretical and experimental investigation of the pigment–protein interactions that enable its function (electronic energy transport). As such, pigment–protein structures are generically used across all photosynthetic organisms for photoconversion, and important lessons about the molecular design principles underpinning the efficiency of these nanoscale "devices" can be learned from studying this complex.

As an important example of this, a potentially new functional aspect of PPCs has recently been revealed in ultrafast nonlinear optical experiments on the FMO complex: the coexistence of surprisingly long-lasting (picosecond) quantum coherence with excitonic energy transfer.[8,9] This has led to a number of new ideas concerning the role of multipigment delocalized states and their temporal coherences in the efficiency of photosynthetic energy funneling.[4,5,8−14] However, because funneling requires a source of dissipation to relax excitations down through the energy landscape,[2,3,15,16] these excited states are subject to significant external noise, most notably from the vibrational and phonon environment of the surrounding protein and water.[3,15,16] Understanding the preservation of quantum dynamics on picosecond time scales in a strongly dephasing environment is currently a subject of intense activity, with increasing appreciation that PPCs are novel open quantum systems in which a clear separation of system and environment interaction strengths and dynamical time scales is absent.[12,15,17−26]

Transport of energy and coherence in these systems requires careful modeling and is qualitatively sensitive to a wide variety of input parameters describing the electronic, optical, and

Received: September 16, 2013
Accepted: November 25, 2013
Published: November 25, 2013

dissipative interactions in the PPC Hamiltonian. The key parameters in this respect are the local pigment transition energies in their binding sites (site energies), couplings between optical transitions in the pigments (excitonic couplings), and the spectral density characterizing the dynamic modulation of site energies and excitonic couplings by the protein.[3,15] These parameters are chosen or extracted according to a variety of theoretical and experimental methods,[27,28] but the large number of free parameters to be extracted, especially when obtained through fitting to optical spectra,[15,29−31] makes the results highly dependent on assumptions made in the modeling. A seemingly more satisfactory method, namely, the ab initio extraction of parameters from purely structural information, that is, the crystal structure, is computationally difficult due to the large number of pigment and protein atoms that interact and contribute to the optical properties.[31,32] Up to now, it has been assumed that to make the problem computationally tractable it is necessary to approximate some, or all, of the PPC by classical, atom-centered point charges.[16,24,31,33] Important issues that arise from such an approach, however, are that mean field charges may not accurately represent the electrostatic environment of the pigment[34] and, in the case of QM/MM simulations, neglect of Pauli repulsion between the pigment and surrounding point charges may lead to distortion of the electronic wave function (the so-called electron leakage problem[27,35]). Ideally, to avoid ambiguity in the choice of classical atomic charges and associated problems with electron leakage and neglect of electronic polarization, a first-principles approach to the determination of the FMO Hamiltonian would be employed, with every atom treated with the same quantum-mechanical level of theory.

In this letter, we present progress toward this goal of a fully ab initio PPC Hamiltonian using recent developments in linear-scaling density functional theory (DFT), as implemented in the ONETEP code, for the computation of excited states. ONETEP combines high basis set accuracy, comparable to that of plane-wave DFT methods, with a computational cost that scales linearly with the number of atoms, which allows for an accurate, fully quantum mechanical description of systems of thousands of atoms,[36] including entire proteins.[37−40] ONETEP describes the single-particle density matrix of a system in terms of in situ optimized local orbitals, referred to as nonorthogonal generalized Wannier functions (NGWFs).[41] These NGWFs are themselves described in terms of a systematic underlying basis,[42] and their form is optimized to describe the local environment of each atom, enabling the method to exhibit systematically convergeable accuracy, equivalent to plane-wave methods.[43] However, local orbitals optimized to describe the occupied part of the density matrix (the valence states) are often poor at describing the unoccupied states of a system. Therefore, Ratcliff et al.[44,45] have recently developed a method whereby a second independent set of so-called "conduction" NGWFs are used to represent a density matrix corresponding to the low-energy unoccupied states. These conduction NGWFs are more delocalized than the valence NGWFs and are ideal for the description of the low-lying unoccupied states of experimental interest, such as those required for calculating optical absorption spectra. By employing Fermi's golden rule in the combined basis, local optical transition energies and densities may be obtained at linear-scaling computational cost.

Under natural illumination conditions and the typical (low) fluences used in optical experiments, only the single-excitation manifold of states needs to be considered to understand linear optical features and energy-transfer dynamics. The excitonic Hamiltonian describing this is given by:

$$H = \sum_i \varepsilon_i |i\rangle\langle i| + \sum_{i\neq j} J_{ij} |i\rangle\langle j| \quad (1)$$

where ε_i is the site energy of the ith BChla of the monomer and J_{ij} is the coherent transfer matrix element between the ith (unexcited) and jth (singly excited) BChlas. We have employed a conceptually straightforward approach to computing parameters of the FMO Hamiltonian, allowing us to estimate site energies and Coulombic couplings from just seven DFT calculations, one centered on each BChla site. Each calculation includes the pigment of interest and all protein residues, BChla pigments, and water molecules that lie within 15 Å (Figure 1).

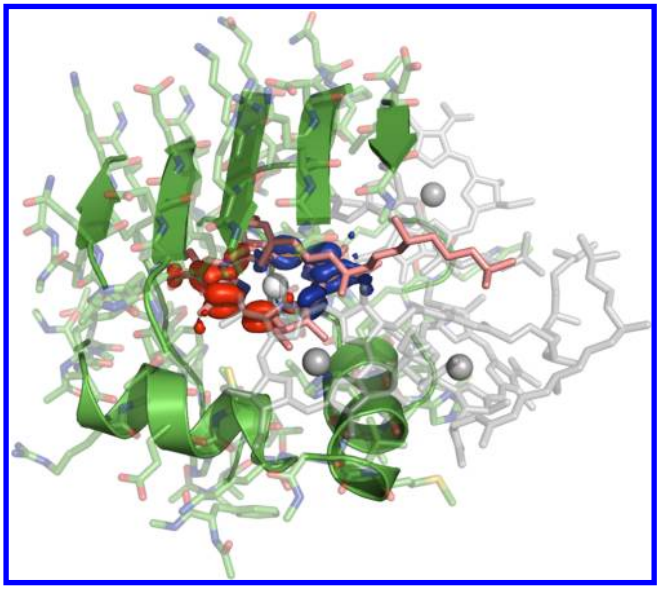

Figure 1. Exemplar 1944-atom cluster used for full QM calculations. The pigment of interest, BChla 4, is shown in pink, with BChlas 3, 5, and 7 in gray and the protein environment in green. The system is embedded in a dielectric medium. Also shown is the BChla 4 transition density as a red/blue isosurface.

The resulting systems range from around 1600 to 2200 atoms, and the largest system studied comprises 6 BChla pigments, 92 protein residues, and 25 water molecules. As discussed in Lever et al.,[46] large-scale DFT calculations of biomolecular clusters should be performed in a dielectric medium to facilitate electronic structure optimization. Hence, we have employed an implicit solvent model[47] with a dielectric constant of 20, which is expected to be a reasonable approximation to the low-temperature dielectric behavior of the solvent used in optical experiments.[16] Importantly, Figure S1 in the Supporting Information shows that the site energies of BChlas 1 and 4 are converged to better than 8 cm^{-1} with respect to the number of atoms included in the simulation. Figure S2 in the Supporting Information reveals that the site energy of BChla 4 varies by <15 cm^{-1} as the dielectric constant of the implicit solvent model is varied in the range 10−80. Together, these results show that at large distances the implicit solvent model is a reasonable approximation to the protein/solvent environment of the pigment.

We have employed the methodology of Ratcliff et al.[44] to optimize localized orbitals describing both occupied and

dx.doi.org/10.1021/jz402000c | J. Phys. Chem. Lett. 2013, 4, 4206−4212

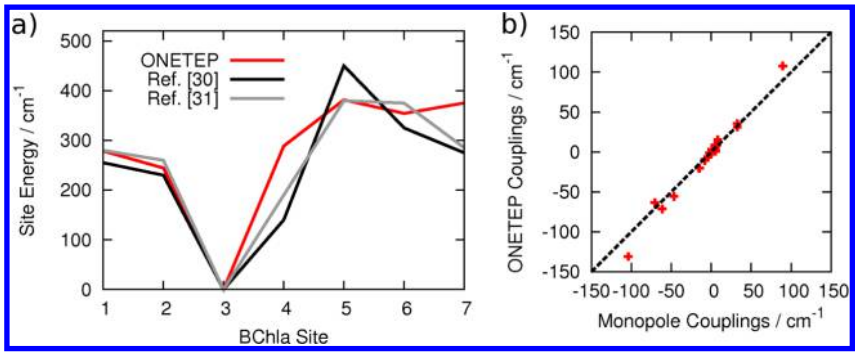

Figure 2. (a) Relative site energies of the seven BChla pigments of the FMO complex, measured by ONETEP. Also shown for comparison are the results of fits to experimental optical spectra by two groups.[30,31] The site energies are shifted such that BChla 3 lies at 0 cm^{-1}. (b) Comparison of excitonic couplings calculated using the ONETEP transition densities in a homogeneous dielectric medium and those calculated from a solution of the Poisson equation using the MEAD software, with the transition densities represented as point charges.[15]

unoccupied states. Site energies and optical matrix elements of the pigment of interest were obtained by projecting out the contributions of NGWFs of all atoms of the BChla pigment. Figure 2a shows that the resulting site energies (ε_i) are in good agreement with widely used site energies that have been fit to reproduce experimental spectra.[30,31] In particular, there is a root-mean-square deviation of just 47 cm^{-1} between our calculated (relative) site energies and those fit to absorption and linear and circular dichroism spectra and their derivatives.[31] Considering the very different approaches employed − one fully QM based on the crystal structure and one fit to experiment with calculated excitonic couplings as input parameters − the agreement is very promising. The identification of BChla 3 as the lowest energy pigment is encouraging given that it appears to be the closest pigment to the reaction center in vivo and is, hence, the most likely candidate for the exit pigment through which excitons leave the complex.[2,28] The main discrepancies between ONETEP and the previous study[31] are in the site energies of BChlas 4 and 7, the implications of which we will return to later.

Part of the benefit of structure-based computational optical spectroscopy is the opportunity to break down contributions to the pigment site energies to determine the microscopic mechanisms by which the protein is able to funnel excitonic energy. Indeed, recent studies have found strong influences from the backbones of two α-helices (labeled α5 and α6) on BChlas 3 and 4 and also that hydrogen bond donors to BChla red shift the site energies by up to ∼130 cm^{-1}.[16,31] We have examined the effects of the residues Tyr 15 and Tyr 345 on the site energies of BChlas 3 and 4, respectively, by mutating the selected residues to alanine and repeating the DFT calculations (Table S1 in the Supporting Information). The hydrogen bond donating Tyr is found to red shift the site energies of the two pigments, by 120 and 129 cm^{-1}, respectively, in good agreement with previous work.[16] Removal of the backbone atoms of helices α5 and α6 is not possible without creating a large number of dangling bonds. Instead, we have computed the effects of replacing the entire helices by a uniform dielectric (Methods in the Supporting Information) on the site energies of BChlas 3 and 4. α5 red shifts BChlas 3 and 4 by 48 and 74 cm^{-1}, respectively, while α6 red shifts BChla 4 by 77 cm^{-1} but has negligible effect on BChla 3.

In a system of pigments with no orbital overlap, excitation energy transfer is mediated by Coulombic coupling between the transition densities of the chromophores.[48,49] We have computed the coupling integral between pigments i and j as:

$$J_{ij} = \frac{1}{\varepsilon}\int \mathrm{d}\mathbf{r}\, \phi_{10}^{(i)}(\mathbf{r})\rho_{10}^{(j)}(\mathbf{r}) \tag{2}$$

where $\rho_{10}^{(j)}(\mathbf{r})$ is the single-particle transition density written in terms of the occupied ($\psi_0^{(j)}$) and unoccupied ($\psi_1^{(j)}$) Kohn−Sham states involved in the optical transition of pigment j:[27,50]

$$\rho_{10}^{(j)}(\mathbf{r}) = \psi_0^{(j)*}(\mathbf{r})\psi_1^{(j)}(\mathbf{r}) \tag{3}$$

and $\phi_{10}^{(i)}(\mathbf{r})$ is the Hartree potential due to the transition density of pigment i. We have computed the dipole moments of the transition densities of each of the seven BChla pigments (Table S3 in the Supporting Information). The magnitudes of the transition dipoles in the protein are site-dependent, ranging from 11.1 D (BChla 7) to 11.6 D (BChla 3). By computing the transition dipole moments using the same DFT methods in vacuum, we compute an average effective dipole strength enhancement (local field correction factor) of 3%, which is due to polarization of the transition density by the protein. So, although eq 2 explicitly includes site-specific polarization of the transition density by the protein environment, it does not include either the optical dielectric screening of the Hartree potential by the environment or the dielectric cavity shape of the BChla pigments, which are both commonly accounted for in excitonic couplings derived from solutions of the inhomogeneous Poisson equation.[15] In the latter case, an optical dielectric constant of 2 has been shown to give a suitable description of PPC environments.[51] A further correction to the computed excitonic couplings must be made here to account for the well-known overestimation of polarizabilty in DFT. Indeed, the average DFT transition dipole moment of the BChla pigments in vacuum (11.1 D) is a factor of 1.8 higher than the experimentally measured value (6.1 D).[52] We have, therefore, included the homogeneous dielectric constant ε as a phenomenological parameter in eq 2 and allowed it to vary. The best agreement of the optical absorption spectrum with experiment is obtained for ε = 4, and it can be shown that this value is in good agreement with the expected optical dielectric of PPCs[51] when overestimation of the polarization, dielectric screening, and cavity shape are taken into account (Supporting Information). Indeed, Figure 2b shows that the correlation between the excitonic couplings computed with the ONETEP transition densities (ε = 4) and those from a previous work, computed using a point charge model in an inhomogeneous dielectric medium (ε = 2),[15] is very good. The main discrepancies are in the couplings between pigment sites 1−2, 5−6, and, to a lesser extent, 3−4, 4−5, and 4−7. The full set of

dx.doi.org/10.1021/jz402000c | J. Phys. Chem. Lett. 2013, 4, 4206−4212

FMO Hamiltonian parameters is shown in Table S2 in the Supporting Information.

From the ab initio PPC Hamiltonian, the linear absorption (LA) spectrum of the FMO complex monomer was computed using simple master equation techniques (Methods in the Supporting Informatiom) and compared, in Figure 3, with the

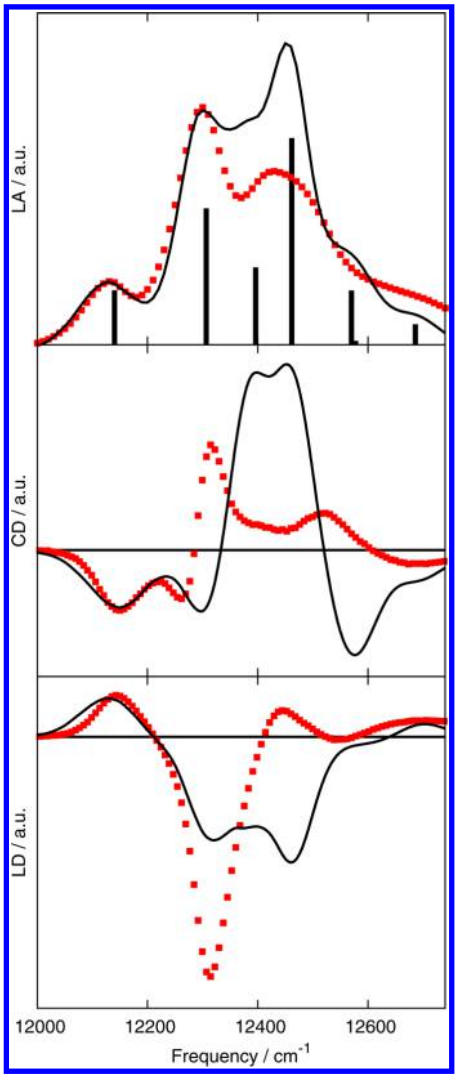

Figure 3. Linear optical absorption (LA), circular dichroism (CD), and linear dichroism (LD) spectra. The experimental spectra are shown as red points[30,53] and the ONETEP spectra are shown as solid black lines. The seven exciton energies, weighted by their dipole moment, are shown as sticks.

experimental spectrum of *P. aestuarii* at T = 77 K.[53] The inhomogeneous disorder was implemented by averaging the spectra over realizations in which each site energy was individually drawn from an independent Gaussian distribution with a defined full width at half-maximum (fwhm) and a mean value equal to the ONETEP-derived site energy shown in Figure 2a. The dissipative background spectral density that determines the excited-state lifetimes and dephasing rates was held constant for each run and was, following the majority of the literature, assumed to be identical on each site. As can be seen, the agreement at low frequencies (covering the first two exciton transitions) is very good and relatively robust with respect to uniform inhomogeneous disorder with fwhm in the range of 40−120 cm^{-1} (Figure S3 in the Supporting Information). These disorder strengths lie in the range typically assumed for FMO and similar PPCs. (Our best fit occurs at a fwhm of 120 cm^{-1}.) However, a significant difference from the experimental spectrum occurs at frequencies in the range of 12 360−12 500 cm^{-1}, with the simulated spectrum showing a larger absorption. An additional peak in the region of 12 580 cm^{-1} is also apparent in the ONETEP spectrum but not in the experimental spectrum.

The higher absorption seen in the simulated spectrum in the region of 12 360−12 500 cm^{-1} can be traced to the eigenvector structure of the ONETEP excitonic Hamiltonian's stationary states (Figure 3, black sticks). The large peak arises from the contribution of exciton 4, which is a strongly delocalized state over sites 3−7 for the values of ε that we consider. The resulting transition dipole moment for this state is coherently enhanced, particularly through the vector addition of the dipoles of sites 4 and 6 (which have the largest weight in the superposition). This gives exciton 4 the largest dipole moment among the exciton transitions. The state itself can be seen to form due to the near degeneracy of the site energies of sites 5, 6, and 7 and the large coupling between sites 5 and 6 (108 cm^{-1}). This leads to lifting of the degeneracy and the formation of strongly delocalized states over these sites, one of which is shifted into near resonance with site 4 and mixes with it to form the large scale superposition that ultimately makes up exciton 4. The structure of this highly delocalized state makes it much more robust to independent site energy disorder,[3] and its inhomogeneous broadening is much weaker than that of the other exciton states. (Disorder approaching the interaction energy scale (∼100 cm^{-1}) is required to significantly alter the state structure.) This combination of properties leads to the large contribution to the absorption spectrum from this state. A further test of the fitness of our ab initio Hamiltonian parameters and the structure of the excitonic states that we obtain is to compare the predicted linear dichroism (LD) and circular dichroism (CD) spectra to the experimental results (Methods in the Supporting Information). Figure 3 shows the comparison with experiment[30] at 77 K for the same uniform disorder and environmental parameters used in the calculation of the LA spectrum. Again, the agreement at low energies, covering the first two transitions, is good for both LD and CD, but a large deviation is again apparent in the region 12 360−12 500 cm^{-1}. At the present, we do not know if this feature in our ONETEP spectra arises from inaccuracies in the site energies of sites 5−7 or the potential inadequacy of the Coulombic coupling calculation for these closely spaced sites.

Figure 4 shows exciton population dynamics obtained from the same master equation calculations for an excitation initially created on site 1 (thought to be one of the two main reception sites for excitons captured by the antenna complexes in green sulfur bacteria). Previous theoretical simulations with a range of other Hamiltonians and spectral functions have found that the relaxation toward the lowest energy exciton state takes place within ∼5 ps,[10−15,21] which is in agreement with the relaxation dynamics we obtain from our ab initio Hamiltonian. Moreover, the structure of our Hamiltonian makes the lowest energy exciton state strongly (>97%) localized on site 3, facilitating the passage of this excitation energy to the next stage of the photosynthetic process (charge separation).

We have demonstrated progress toward an ab initio parametrization of PPC Hamiltonians for optical absorption spectra of large-scale biological systems using linear-scaling

dx.doi.org/10.1021/jz402000c | *J. Phys. Chem. Lett.* 2013, 4, 4206−4212

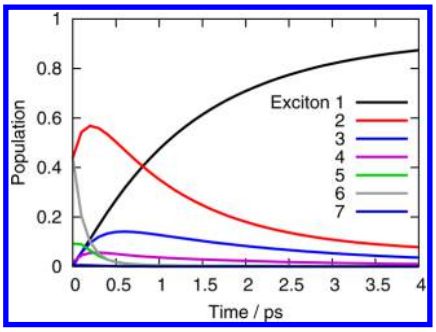

Figure 4. Exciton occupation probability dynamics. Population transfer to the lowest energy eigenstate occurs within 4 to 5 ps at T = 77 K.

density functional theory techniques. In ONETEP, separately optimizing valence and conduction state NGWFs in situ allows for a minimal number of atom-centered orbitals to be used while maintaining near-complete basis set accuracy for the computation of local optical transition energies. Starting only with the FMO atomic coordinates as input, we have extracted clusters centered on each of the BChla pigments and calculated both their site energies and interpigment Coulombic coupling matrix elements, both of which are in broad agreement with previous data extracted from theory and experiment.[15,30,31] It was demonstrated, for BChlas 3 and 4, that pigment−protein hydrogen bonds red shift the site energies, in good agreement with previous studies.[16,31]

We emphasize that by simulating the entire cluster of ∼2000 atoms at the same level of quantum mechanical theory we remove the need to introduce classical point charges into our simulations, which in turn reduces errors in the description of the electrostatic environment of the pigments[34] and allows for site-specific transition densities. In comparison with QM/MM simulations, there are no issues related to electron leakage, which may distort the calculated transition density. Indeed, recalculation of the site energies within ONETEP at the same level of theory, but representing the protein environment as a background of classical point charges,[54] gives a root-mean-square error of 107 cm^{-1} in comparison with the full DFT results (Supporting Information).

Despite these important steps toward a fully ab initio PPC Hamiltonian, it has been necessary to include a number of assumptions and phenomenological parameters. It is well known that Kohn−Sham DFT in conjunction with the PBE exchange-correlation functional systematically underestimates the HOMO−LUMO gap and overestimates polarizabilities. We have uniformly shifted the calculated site energies to align the optical spectra with experiment and have included an effective dielectric in our calculation of the Coulombic couplings (eq 2) to compensate for these errors. We have neglected the effects of nuclear polarization within the explicitly modeled QM clusters on the calculated site energies, which is reasonable given the small expected reorganization energy associated with the Q_y transition in BChla.[16] Outside the QM clusters, we have approximated the electrostatic environment by an implicit solvent model with a dielectric constant of 20, which facilitates electronic structure convergence.[46] The low-temperature dielectric behavior of the solvent and protein is open to debate, but we cannot rule out changes in relative site energies if smaller dielectric constants are used to represent the protein, as is common in methods employing classical point charges.[16,27] Future studies into the effects of environment-dependent dielectric constants or explicitly representing the entire FMO monomer with DFT would resolve this question. Although the PPC structures used here have been obtained from a high-resolution X-ray crystal structure,[7] further tuning of the relative site energies by full ab initio optimization of the extracted clusters cannot be ruled out and should be the focus of future development efforts. We have employed Fermi's golden rule to compute local optical transition energies, which will remain valid as long as the population of the initial state is not strongly depleted by scattering, as would be the case in a realistic biological environment. Nevertheless, improvements in accuracy are expected when considering a time-dependent (TD) Hamiltonian, and recent advances in linear-scaling TD-DFT will allow further development in this respect.[55] Finally, the absorption linewidths of the calculated spectra are sensitive to the frequency structure of the spectral function and especially to its form near zero frequency (which determines the effective pure dephasing rate).[21] We hope that providing methods to derive an accurate ab initio excitonic Hamiltonian will facilitate increasingly rigorous first-principles or experimental determination of the real spectral functions, which are essential for investigating quantum dynamics in these light-harvesting complexes.

■ COMPUTATIONAL METHODS

Calculations were based on the *holo* (8 BChla per monomer) form of the trimeric 1.3 Å X-ray crystal structure of *Prosthecochloris aestuarii* (PDB: 3EOJ).[7] DFT calculations were performed with the ONETEP code, using the PBE exchange-correlation functional. We have used a smeared ion representation under open-boundary conditions with a relative dielectric of 20.[47,56] Optical spectra were calculated from Fermi's golden rule in a joint valence and conduction basis.[44] Note that the current method of conduction NGWF optimization is suitable only for describing unoccupied states that are localized on the system and do not hybridize significantly with the continuum of higher-energy unbound states. However, these are the states of interest for most properties because transitions to the continuum of unbound states do not have large optical matrix elements and are thus, in general, optically dark. A convenient local decomposition of the density of states and optical spectrum can be obtained by harnessing the fact that the description of the electronic structure employs atom-centered local orbitals.[57] A projector $\Sigma_{\alpha\in I}|\phi_\alpha\rangle\langle\phi^\alpha|$ can be inserted into the density of states expression and into one of the terms of the optical matrix element to project out the contributions from NGWFs α of all of the atoms I of a particular group, in this case, a single BChla molecule. The Hartree potential due to the transition density for the calculation of Coulombic couplings was calculated in a 90 Å cell (large enough to enclose all BChla pigments and their transition densities) using a multigrid approach with open boundary conditions in vacuum.[47] The coupling integral was evaluated on a grid with spacing 0.225 Bohr. Full details of the computational model, ONETEP parameters, and spectral calculations may be found in the Supporting Information.

■ ASSOCIATED CONTENT

Ⓢ Supporting Information

Supporting methods, convergence of site energies (with system size, implicit solvent dielectric, and ONETEP parameters), effect of specific pigment−protein interactions on site energies, full PPC Hamiltonian parameters, effect of decreasing spectral

density disorder, discussion of the optical dielectric constant, and comparison between QM/MM and full QM site energies. This material is available free of charge via the Internet at http://pubs.acs.org.

AUTHOR INFORMATION

Corresponding Author

*E-mail: djc56@cam.ac.uk.

Notes

The authors declare no competing financial interest.

ACKNOWLEDGMENTS

We are grateful to Dugan Hayes (Engel Group, U. Chicago) for providing the experimental absorption spectrum data used for comparison in this work, Rienk van Grondelle and Markus Wendling for experimental LD and CD spectra, Sangwoo Shim and Alán Aspuru-Guzik for providing BChla force field parameters, and Tobias Kramer for spectral density parameters (not ultimately used). Computational resources were provided by the Cambridge HPC Service, funded by EPSRC Grant EP/J017639/1. D.J.C. is supported by a Marie Curie International Outgoing Fellowship within the seventh European Community Framework Programme. A.W.C. and N.D.M.H. acknowledge support from the Winton Programme for the Physics of Sustainability.

REFERENCES

(1) Olson, J. M. *Discoveries in Photosynthesis*; Springer: Netherlands, 2005.

(2) Blankenship, R. E. *Molecular Mechanisms of Photosynthesis*; Blackwell Science Ltd: Oxford, U.K., 2008.

(3) Van Amerongen, H.; Valkūnas, L.; Van Grondelle, R. *Photosynthetic Excitons*; World Scientific: Singapore, 2000.

(4) Scholes, G. D.; Fleming, G. R.; Olaya-Castro, A.; van Grondelle, R. Lessons from Nature about Solar Light Harvesting. *Nat. Chem.* **2011**, *3*, 763−774.

(5) Lambert, N.; Chen, Y.-N.; Cheng, Y.-C.; Li, C.-M.; Chen, G.-Y.; Nori, F. Quantum Biology. *Nat. Phys.* **2012**, *9*, 10−18.

(6) Creatore, C.; Parker, M.; Emmott, S.; Chin, A. An Efficient Biologically-Inspired Photocell Enhanced by Quantum Coherence. arXiv:1307.5093, 2013.

(7) Tronrud, D. E.; Wen, J.; Gay, L.; Blankenship, R. E. The Structural Basis for the Difference in Absorbance Spectra for the FMO Antenna Protein from Various Green Sulfur Bacteria. *Photosynth. Res.* **2009**, *100*, 79−87.

(8) Engel, G. S.; Calhoun, T. R.; Read, E. L.; Ahn, T.-K.; Mančal, T.; Cheng, Y.-C.; Blankenship, R. E.; Fleming, G. R. Evidence for Wavelike Energy Transfer through Quantum Coherence in Photosynthetic Systems. *Nature* **2007**, *446*, 782−786.

(9) Panitchayangkoon, G.; Hayes, D.; Fransted, K. A.; Caram, J. R.; Harel, E.; Wen, J.; Blankenship, R. E.; Engel, G. S. Long-Lived Quantum Coherence in Photosynthetic Complexes at Physiological Temperature. *Proc. Natl. Acad. Sci. U.S.A.* **2010**, *107*, 12766−12770.

(10) Mohseni, M.; Rebentrost, P.; Lloyd, S.; Aspuru-Guzik, A. Environment-Assisted Quantum Walks in Photosynthetic Energy Transfer. *J. Chem. Phys.* **2008**, *129*, 174106−174106.

(11) Plenio, M. B.; Huelga, S. F. Dephasing-Assisted Transport: Quantum Networks and Biomolecules. *New J. Phys.* **2008**, *10*, 113019.

(12) Ishizaki, A.; Fleming, G. R. Theoretical Examination of Quantum Coherence in a Photosynthetic System at Physiological Temperature. *Proc. Natl. Acad. Sci. U.S.A.* **2009**, *106*, 17255−17260.

(13) Caruso, F.; Chin, A. W.; Datta, A.; Huelga, S. F.; Plenio, M. B. Highly Efficient Energy Excitation Transfer in Light-Harvesting Complexes: The Fundamental Role of Noise-Assisted Transport. *J. Chem. Phys.* **2009**, *131*, 105106−105106.

(14) Rebentrost, P.; Mohseni, M.; Kassal, I.; Lloyd, S.; Aspuru-Guzik, A. Environment-Assisted Quantum Transport. *New J. Phys.* **2009**, *11*, 033003.

(15) Adolphs, J.; Renger, T. How Proteins Trigger Excitation Energy Transfer in the FMO Complex of Green Sulfur Bacteria. *Biophys. J.* **2006**, *91*, 2778−2797.

(16) Müh, F.; Madjet, M. E.; Adolphs, J.; Abdurahman, A.; Rabenstein, B.; Ishikita, H.; Knapp, E. W.; Renger, T. α-Helices Direct Excitation Energy Flow in the Fenna-Matthews-Olson Protein. *Proc. Natl. Acad. Sci. U.S.A.* **2007**, *104*, 16862−16867.

(17) Thorwart, M.; Eckel, J.; Reina, J. H.; Nalbach, P.; Weiss, S. Enhanced Quantum Entanglement in the Non-Markovian Dynamics of Biomolecular Excitons. *Chem. Phys. Lett.* **2009**, *478*, 234−237.

(18) Roden, J.; Eisfeld, A.; Wolff, W.; Strunz, W. T. Influence of Complex Exciton-Phonon Coupling on Optical Absorption and Energy Transfer of Quantum Aggregates. *Phys. Rev. Lett.* **2009**, *103*, 058301.

(19) Prior, J.; Chin, A. W.; Huelga, S. F.; Plenio, M. B. Efficient Simulation of Strong System-Environment Interactions. *Phys. Rev. Lett.* **2010**, *105*, 050404.

(20) Renger, T.; Klinger, A.; Steinecker, F.; Schmidt am Musch, M.; Numata, J.; Müh, F. Normal Mode Analysis of the Spectral Density of the Fenna-Matthews-Olson Light-Harvesting Protein: How the Protein Dissipates the Excess Energy of Excitons. *J. Phys. Chem. B* **2012**, *116*, 14565−14580.

(21) Kreisbeck, C.; Kramer, T. Long-Lived Electronic Coherence in Dissipative Exciton Dynamics of Light-Harvesting Complexes. *J. Phys. Chem. Lett.* **2012**, *3*, 2828−2833.

(22) Kolli, A.; O'Reilly, E. J.; Scholes, G. D.; Olaya-Castro, A. The Fundamental Role of Quantized Vibrations in Coherent Light Harvesting by Cryptophyte Algae. *J. Chem. Phys.* **2012**, *137*, 174109−174109.

(23) Christensson, N.; Kauffmann, H. F.; Pullerits, T.; Mančal, T. Origin of Long-Lived Coherences in Light-Harvesting Complexes. *J. Phys. Chem. B* **2012**, *116*, 7449−7454.

(24) Shim, S.; Rebentrost, P.; Valleau, S.; Aspuru-Guzik, A. Atomistic Study of the Long-Lived Quantum Coherences in the Fenna-Matthews-Olson Complex. *Biophys. J.* **2012**, *102*, 649−660.

(25) Tiwari, V.; Peters, W. K.; Jonas, D. M. Electronic Resonance with Anticorrelated Pigment Vibrations Drives Photosynthetic Energy Transfer Outside the Adiabatic Framework. *Proc. Natl. Acad. Sci. U.S.A.* **2013**, *110*, 1203−1208.

(26) Chin, A.; Prior, J.; Rosenbach, R.; Caycedo-Soler, F.; Huelga, S.; Plenio, M. The Role of Non-Equilibrium Vibrational Structures in Electronic Coherence and Recoherence in Pigment-Protein Complexes. *Nat. Phys.* **2013**, *9*, 113−118.

(27) Renger, T.; Müh, F. Understanding Photosynthetic Light-Harvesting: A Bottom Up Theoretical Approach. *Phys. Chem. Chem. Phys.* **2013**, *15*, 3348−3371.

(28) Milder, M. T. W.; Brüggemann, B.; van Grondelle, R.; Herek, J. L. Revisiting the Optical Properties of the FMO Protein. *Photosynth. Res.* **2010**, *104*, 257−274.

(29) Louwe, R. J. W.; Vrieze, J.; Hoff, A. J.; Aartsma, T. J. Toward an Integral Interpretation of the Optical Steady-State Spectra of the FMO-Complex of Prosthecochloris Aestuarii. 2. Exciton Simulations. *J. Phys. Chem. B* **1997**, *101*, 11280−11287.

(30) Wendling, M.; Przyjalgowski, M. A.; Gülen, D.; Vulto, S. I. E.; Aartsma, T. J.; van Grondelle, R.; van Amerongen, H. The Quantitative Relationship between Structure and Polarized Spectroscopy in the FMO Complex of Prosthecochloris Aestuarii: Refining Experiments and Simulations. *Photosynth. Res.* **2002**, *71*, 99−123.

(31) Adolphs, J.; Müh, F.; Madjet, M. E.; Renger, T. Calculation of Pigment Transition Energies in the FMO Protein. *Photosynth. Res.* **2008**, *95*, 197−209.

(32) Adolphs, J.; Müh, F.; Madjet, M. E.; Schmidt am Busch, M.; Renger, T. Structure-Based Calculations of Optical Spectra of Photosystem I Suggest an Asymmetric Light-Harvesting Process. *J. Am. Chem. Soc.* **2010**, *132*, 3331−3343.

(33) Olbrich, C.; Jansen, T. L. C.; Liebers, J.; Aghtar, M.; Strumpfer, J.; Schulten, K.; Knoester, J.; Kleinekathofer, U. From Atomistic Modeling to Excitation Transfer and Two-Dimensional Spectra of the FMO Light-Harvesting Complex. *J. Phys. Chem. B* **2011**, *115*, 8609−8621.
(34) Lee, L. P.; Cole, D. J.; Skylaris, C.-K.; Jorgensen, W. L.; Payne, M. C. Polarized Protein-Specific Charges from Atoms-in-Molecule Electron Density Partitioning. *J. Chem. Theory Comput.* **2013**, *9*, 2981−2991.
(35) Neugebauer, J. Subsystem-Based Theoretical Spectroscopy of Biomolecules and Biomolecular Assemblies. *Chem. Phys. Chem.* **2009**, *10*, 3148−3173.
(36) Hine, N. D. M.; Haynes, P. D.; Mostofi, A. A.; Skylaris, C. K.; Payne, M. C. Linear-Scaling Density-Functional Theory with Tens of Thousands of Atoms: Expanding the Scope and Scale of Calculations with ONETEP. *Comput. Phys. Commun.* **2009**, *180*, 1041−1053.
(37) Lee, L. P.; Cole, D. J.; Payne, M. C.; Skylaris, C.-K. Natural Bond Orbital Analysis in the ONETEP Code: Applications to Large Protein Systems. *J. Comput. Chem.* **2013**, *34*, 429−444.
(38) Cole, D. J.; O'Regan, D. D.; Payne, M. C. Ligand Discrimination in Myoglobin from Linear-Scaling DFT+U. *J. Phys. Chem. Lett.* **2012**, *3*, 1448−1452.
(39) Cole, D. J.; Rajendra, E.; Roberts-Thomson, M.; Hardwick, B.; McKenzie, G. J.; Payne, M. C.; Venkitaraman, A. R.; Skylaris, C. K. Interrogation of the Protein-Protein Interactions between Human BRCA2 BRC Repeats and RAD51 Reveals Atomistic Determinants of Affinity. *PLoS Comput. Biol.* **2011**, *7*, e1002096.
(40) Cole, D. J.; Skylaris, C. K.; Rajendra, E.; Venkitaraman, A. R.; Payne, M. C. Protein-Protein Interactions from Linear-Scaling First-Principles Quantum-Mechanical Calculations. *Europhys. Lett.* **2010**, *91*, 37004.
(41) Skylaris, C. K.; Mostofi, A. A.; Haynes, P. D.; Dieguez, O.; Payne, M. C. The Non-Orthogonal Generalised Wannier Function Pseudopotential Plane-Wave Method. *Phys. Rev. B* **2002**, *66*, 035119.
(42) Mostofi, A. A.; Haynes, P. D.; Skylaris, C. K.; Payne, M. C. Preconditioned Iterative Minimisation for Linear-Scaling Electronic Structure Calculations. *J. Chem. Phys.* **2003**, *119*, 8842−8848.
(43) Skylaris, C. K.; Haynes, P. D. Achieving Plane Wave Accuracy in Linear-Scaling Density Functional Theory Applied to Periodic Systems: A Case Study on Crystalline Silicon. *J. Chem. Phys.* **2007**, *127*, 164712.
(44) Ratcliff, L. E.; Hine, N. D. M.; Haynes, P. D. Calculating Optical Absorption Spectra for Large Systems using Linear-Scaling Density-Functional Theory. *Phys. Rev. B* **2011**, *84*, 165131.
(45) Ratcliff, L. E.; Haynes, P. D. Ab Initio Calculations of the Optical Absorption Spectra of C60-Conjugated Polymer Hybrids. *Phys. Chem. Chem. Phys.* **2013**, *15*, 13024−13031.
(46) Lever, G.; Cole, D. J.; Hine, N. D. M.; Haynes, P. D.; Payne, M. C. Electrostatic Considerations Affecting the Calculated HOMO-LUMO Gap in Protein Molecules. *J. Phys.: Condens. Matter* **2013**, *25*, 152101.
(47) Dziedzic, J.; Helal, H. H.; Skylaris, C.-K.; Mostofi, A. A.; Payne, M. C. Minimal Parameter Implicit Solvent Model for ab Initio Electronic Structure Calculations. *Europhys. Lett.* **2011**, *95*, 43001.
(48) Krueger, B. P.; Scholes, G. D.; Fleming, G. R. Calculation of Couplings and Energy-Transfer Pathways between the Pigments of LH2 by the ab Initio Transition Density Cube Method. *J. Phys. Chem. B* **1998**, *102*, 5378−5386.
(49) Renger, T.; Müh, F. Theory of Excitonic Couplings in Dielectric Media. *Photosynth. Res.* **2012**, *111*, 47−52.
(50) Madjet, M. E.; Abdurahman, A.; Renger, T. Intermolecular Coulomb Couplings from ab Initio Electrostatic Potentials: Application to Optical Transitions of Strongly Coupled Pigments in Photosynthetic Antennae and Reaction Centers. *J. Phys. Chem. B* **2006**, *110*, 17268−17281.
(51) Renger, T.; Madjet, M. E.; Müh, F.; Trostmann, I.; Schmitt, F.-J.; Theiss, C.; Paulsen, H.; Eichler, H. J.; Knorr, A.; Renger, G. Thermally Activated Superradiance and Intersystem Crossing in the Water-Soluble Chlorophyll Binding Protein. *J. Phys. Chem. B* **2009**, *113*, 9948−9957.
(52) Knox, R. S.; Spring, B. Q. Dipole Strengths in the Chlorophylls. *Photochem. Photobiol.* **2003**, *77*, 497−501.
(53) Hayes, D.; Engel, G. S. Extracting the Excitonic Hamiltonian of the Fenna-Matthews-Olson Complex using Three-Dimensional Third-Order Electronic Spectroscopy. *Biophys. J.* **2011**, *100*, 2043−2052.
(54) Fox, S. J.; Pittock, C.; Fox, T.; Tautermann, C.; Malcolm, N.; Skylaris, C.-K. Electrostatic Embedding in Large-Scale First Principles Quantum Mechanical Calculations on Biomolecules. *J. Chem. Phys.* **2011**, *135*, 224107.
(55) Zuehlsdorff, T. J.; Hine, N. D. M.; Spencer, J. S.; Harrison, N. M.; Riley, D. J.; Haynes, P. D. Linear-Scaling Time-Dependent Density-Functional Theory in the Linear Response Formalism. *J. Chem. Phys.* **2013**, *139*, 064104.
(56) Hine, N. D. M.; Dziedzic, J.; Haynes, P. D.; Skylaris, C. K. Electrostatic Interactions in Finite Systems Treated with Periodic Boundary Conditions: Application to Linear-Scaling Density Functional Theory. *J. Chem. Phys.* **2011**, *135*, 204103.
(57) Hine, N. D. M.; Avraam, P. W.; Tangney, P.; Haynes, P. D. Linear-Scaling Density Functional Theory Simulations of Polar Semiconductor Nanorods. *J. Phys.: Conf. Ser.* **2012**, *367*, 012002.